PAPER

Comparison of ±σ-hole and ±R·-hole interactions formed by tetrel-containing complexes: a computational study†

Mahmoud A. A. Ibrahim [iD]* and Ebtisam M. Z. Telb

For the first time, unconventional ±R·-hole interactions were unveiled in tetrel-containing complexes. The nature and characteristics of ±R·-hole interactions were explored relative to their ±σ-hole counterparts for ·TF₃··· and W–T–F₃···B/R·/A complexes (where T = C, Si, and Ge, W = H and F, B = Lewis bases, R· = free radicals, and A = Lewis acids). In an effort to thoroughly investigate such interactions, a plethora of quantum mechanical calculations, including molecular electrostatic potential (MEP), maximum positive electrostatic potential ($V_{s,max}$), point-of-charge (PoC), interaction energy, symmetry adapted perturbation theory (SAPT), and reduced density gradient–noncovalent interaction (RDG–NCI) calculations, were applied. The most notable findings to emerge from this study are that (i) from the electrostatic perspective, the molecular stabilization energies of ·TF₃ and W–T–F₃ monomers became more negative as the Lewis basicity increased, (ii) the most stable complexes were observed for the ones containing Lewis bases, forming ⁻σ-hole and ⁻R·-hole interactions, and the interaction energies systematically increased in the order H–T–F₃···B < ·TF₃···B < F–T–F₃···B, (iii) contrariwise, the ⁺σ-hole and ⁺R·-hole interactions with Lewis acids are more energetically favorable in the order F–T–F₃···A < ·TF₃···A < H–T–F₃···A, and (iv) generally, the dispersion force plays a key role in stabilizing the tetrel-containing complexes, jointly with the electrostatic and induction forces for the interactions with Lewis bases and acids, respectively. Concretely, the findings presented in this paper add to our understanding of the characteristics and nature of such intriguing interactions.

1. Introduction

σ-Hole interaction is a major area of interest within the realm of noncovalent interactions owing to its primordial roles in molecular recognition,[1,2] crystal materials,[3,4] and biological systems.[5,6] Accordingly, researchers have focused more attention on its characteristics and nature which have been widely studied from both computational and experimental aspects.[7–11] These studies collectively proclaimed a series of different types of σ-hole-based interactions—namely, tetrel[12,13] pnicogen[14,15] chalcogen[16,17] halogen[18,19] and aerogen bonds[20,21] embracing the Group IV–VIII elements, respectively. The σ-hole interactions can be traced back to the presence of a positive or less negative region along the extension of the covalently bonded Group IV–VIII elements (termed a σ-hole).[22–24]

Among the σ-hole interactions, tetrel bonding has received immense interest due to its technological and fundamental magnitude in supramolecular chemistry[25] and dynamical processes such as protein folding and ligand–acceptor

interactions.[26,27] Several studies have documented the potentiality of the tetrel-containing molecules to form ⁻σ-hole interactions as a consequence of the interaction of Group IV elements (T) *via* the σ-hole with Lewis bases (B) such as lone-pair (lp),[28–31] anion,[32,33] π-systems.[34,35] Recently, a thought-provoking study has given prominence to ⁺σ-hole interactions of tetrel-containing complexes, which demonstrated the ability of tetrel-containing molecules to preferentially interact with Lewis acids (A).[30] Nonetheless, only a handful of reports in the literature were introduced to investigate the intermolecular interactions of tetrel-containing molecules with Lewis acids.

In light of recent research, single-electron noncovalent interactions were reported, referring to an interaction between the unpaired electron of a radical (R·) acting as a Lewis base and the σ-hole on the Group IV–VIII elements acting as a Lewis acid.[36–44] Considering the pivotal role of radicals in combustion, polymerization, biochemistry, and many other chemical processes,[45–48] further studies are needed to characterize the interactions of radical species with tetrel-containing molecules.

One of the most significant current investigations in noncovalent interactions is that ascribed to the lp-hole. Lp-hole interactions were accentuated for Group V–VIII elements as a result of a positive region opposite to the lp (called lp-hole).[49–51] According to the term lp-hole, it is not plausible for

Computational Chemistry Laboratory, Chemistry Department, Faculty of Science, Minia University, Minia 61519, Egypt. E-mail: m.ibrahim@compchem.net

sp^3-hybridized tetrel-containing molecules to form this type of interaction. A question has been raised about whether sp^3-hybridized tetrel radicals ($^{\bullet}$TX$_3$) can form another intriguing interaction so-called R$^{\bullet}$-hole interaction. This interaction is attributed to the presence of a positive region opposite to the unpaired electron on the tetrel (termed, R$^{\bullet}$-hole). As far as our knowledge extends, no previous study has assessed the occurrence of R$^{\bullet}$-hole interaction.

Subsequently, the objectives of the current work were to (i) uncover the occurrence of the R$^{\bullet}$-hole interactions and (ii) gain insight into the characteristics and nature of the σ-hole and R$^{\bullet}$-hole interactions of tetrel-containing molecules with Lewis bases, free radicals, and Lewis acids. $^{-}$R$^{\bullet}$-hole and $^{+}$R$^{\bullet}$-hole interactions were assigned for the interactions with Lewis bases and acids, by analogy with $^{-}$σ-hole and $^{+}$σ-hole interactions, respectively. The point-of-charge (PoC) approach was utilized to precisely determine the R$^{\bullet}$-hole location and elucidate the $^{\pm}$σ-hole and $^{\pm}$R$^{\bullet}$-hole interactions from the electrostatic perspective.[30,49,52–56] The interaction energies for $^{\bullet}$TF$_3$··· and W–T–F$_3$···B/R$^{\bullet}$/A complexes (where T = C, Si, and Ge, and W = H and F) were calculated at the MP2/aug-cc-pVTZ(PP) and CCSD(T)/CBS levels of theory. The symmetry adapted perturbation theory (SAPT) and reduced density gradient–noncovalent interaction (RDG–NCI) index calculations were executed to reconnoiter the characteristics and nature of such interactions. This study makes a major contribution to research on tetrel radicals-bonded complexes by demonstrating the characteristics and nature of R$^{\bullet}$-hole interactions compared to the σ-hole ones for the first time.

2. Computational methods

In the current study, $^{\bullet}$TF$_3$ and W–T–F$_3$ model systems were chosen as a case study to investigate the σ-hole and R$^{\bullet}$-hole interactions with Lewis bases, acids, and free radicals (where T = C, Si, and Ge, and W = H and F). NCH and FH molecules were investigated as Lewis bases and acids, while free radicals were exemplified by $^{\bullet}$CH$_3$ and $^{\bullet}$CF$_3$. The geometries of the systems were initially optimized at the MP2/aug-cc-pVTZ level of theory, with treating Ge atom with aug-cc-pVTZ-PP basis set to account for relativistic effects.[57–59] The molecular electrostatic potential (MEP)

maps were generated for the optimized monomers and then mapped on 0.002 au electron density contours based on the previous recommendations.[24,60] Moreover, the maximum positive electrostatic potential ($V_{s,max}$) calculations at σ-hole and R$^{\bullet}$-hole locations were carried out using the Multiwfn3.7 software.[61]

To fulfill the aim of this investigation, the R$^{\bullet}$-hole location was first precisely determined. The studied $^{\bullet}$TF$_3$ radicals were aligned to the x-axis, and the yz plane was then scanned by −0.01 au PoC with a step size of 0.1 Å, using the point-of-charge (PoC) approach (Fig. 1(ia)). The PoC was placed at a distance of 2.0 Å from the tetrel atom and moved along both y- and z-directions in a range from 1.6 to −1.6 Å, generating 2D-molecular stabilization energy surfaces (see Fig. 1(ia)). To inspect the effect of Lewis basicity and acidity on the $^{\pm}$σ-hole and $^{\pm}$R$^{\bullet}$-hole interactions strength, different values of negatively and positively charged points stimulating Lewis bases and acids, respectively, were applied. In the latter calculation, the studied monomers were aligned to the x-axis, and the T···PoC distance effect on the strength of interaction was evaluated in the range 2.5 to 5.0 Å (see Fig. 1(ib)). The employed PoC values were set to ±0.10, ±0.25, ±0.50, and ±1.00 au. The strength of the $^{\pm}$σ-hole and $^{\pm}$R$^{\bullet}$-hole interactions was estimated at MP2/aug-cc-pVTZ(PP) level of theory in terms of the molecular stabilization energy ($E_{stablization}$) according to the following equation:[30,49,50,52–56]

$$E_{stablization} = E_{tetrel\text{-}containing\ molecule\cdots PoC} - E_{tetrel\text{-}containing\ molecule}$$

To analyze the potentiality of $^{\bullet}$TF$_3$ and W–T–F$_3$ systems to favorably interact via the σ-hole and R$^{\bullet}$-hole with B, R$^{\bullet}$, and A (see Fig. 1(ii)), full geometrical optimization of the complexes in C_{3V} space group was performed at the MP2/aug-cc-pVTZ level of theory (with PP functions for Ge atom). Vibrational frequency calculations were not performed for the binary complexes; thus, there was a possibility that the structures were not energetic minima. The interaction energies of the binary complexes were then estimated at the same level of optimization and performed with taking basis set superposition error (BSSE) correction into account.[62] The interaction energies were computed as the difference in energy between the complex and the sum of monomers with the same geometries as in the complex. The
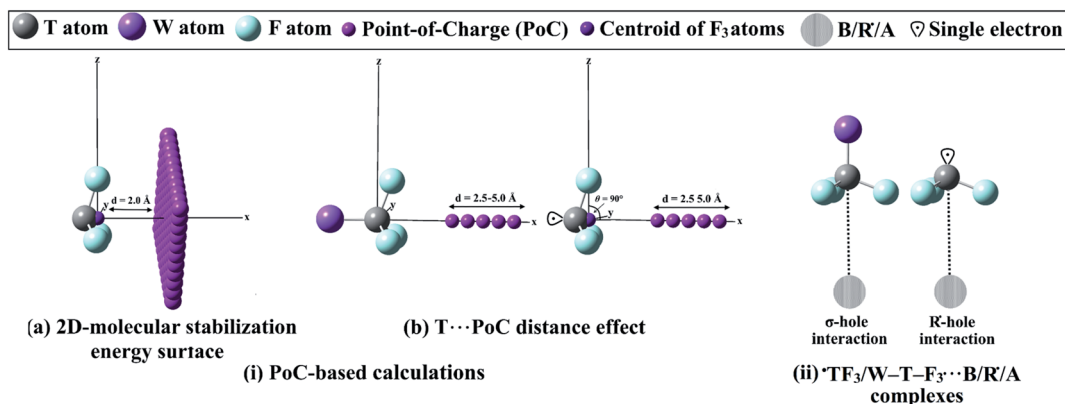

Fig. 1 Schematic representation of (i) implemented PoC-based calculations and (ii) $^{\bullet}$TF$_3$··· and W−T−F3···B/R$^{\bullet}$/A complexes.

frozen-core (FC) approximation was adopted for all MP2 calculations. Furthermore, the interaction energies were calculated for the optimized complexes at the CCSD(T)/CBS level of theory. The CCSD(T)/CBS energies were calculated based on the following equation:[63]

$$E_{CCSD(T)/CBS} = \Delta E_{MP2/CBS} + \Delta E_{CCSD(T)}$$

where:

$$\Delta E_{MP2/CBS} = (64E_{MP2/aug\text{-}cc\text{-}pVQZ} - 27E_{MP2/aug\text{-}cc\text{-}pVTZ})/37$$

$$\Delta E_{CCSD(T)} = E_{CCSD(T)/aug\text{-}cc\text{-}pVdZ} - E_{MP2/aug\text{-}cc\text{-}pVDZ}$$

To have a more in-depth insight into the nature of σ-hole and R˙-hole interactions, the energy decomposition calculations were performed through the symmetry adapted perturbation theory-based energy decomposition analysis (SAPT-EDA)

method using PSI4 code.[64,65] The SAPT-EDA method provides a separation of interaction energies into four physically meaningful components, such as those arising from electrostatics (E_{elst}), exchange (E_{exch}), induction (E_{ind}), and dispersion (E_{disp}). The interaction energies were estimated at SAPT0 truncation along with an aug-cc-pVTZ basis set, given as follows:[66–68]

$$E_{int}^{SAPT0} = E_{elst} + E_{exch} + E_{ind} + E_{disp}$$

where:

$$E_{elst} = E_{elst}^{(10)}$$

$$E_{exch} = E_{exch}^{(10)}$$

$$E_{ind} = E_{ind,resp}^{(20)} + E_{exch\text{-}ind,resp}^{(20)} + \delta E_{HF}^{(2)}$$

$$E_{disp} = E_{disp}^{(20)} + E_{exch\text{-}disp}^{(20)}$$

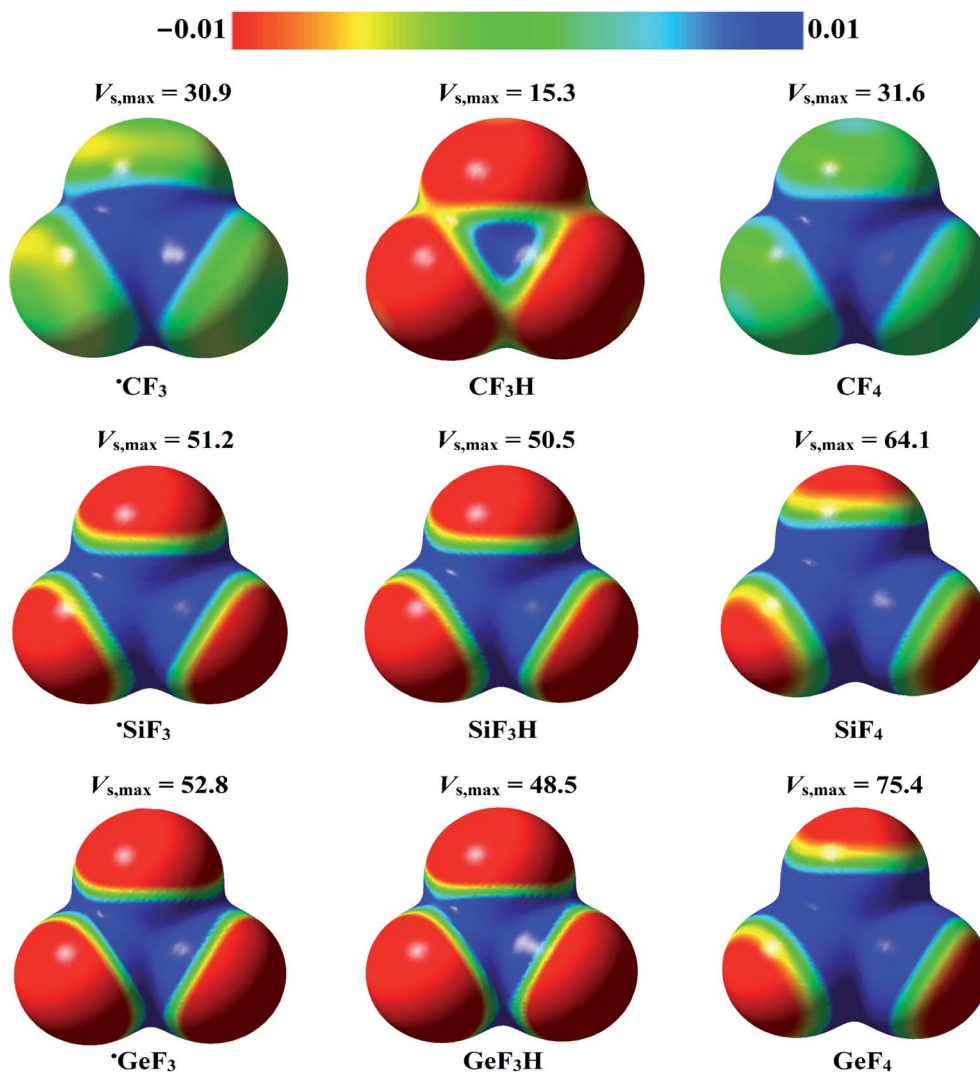**Fig. 2** Molecular electrostatic potential (MEP) maps of the investigated ˙TF$_3$ and W−T−F$_3$ systems (where T = C, Si, and Ge, and W = H and F) plotted at 0.002 au electron density contours. The electrostatic potentials vary from −0.01 au (red) to 0.01 au (blue). The calculated maximum positive electrostatic potential ($V_{s,max}$, kcal mol^{-1}) at the σ-hole and R˙-hole are also depicted.

To analyze the bonding characteristics of σ-hole and R˙-hole interactions, reduced density gradient–noncovalent interaction (RDG–NCI) indices were constructed, and the NCI plots were also illustrated.[69] The gradient isosurfaces were colored on a blue-green-red (BGR) scale, where blue surfaces refer to strong attractions, green surfaces show weak interactions, and red surfaces imply strong repulsions. The coloring scale of electron density (ρ) was from −0.035 (blue) to 0.020 (red) au. The RDG–NCI analysis was carried out using Multiwfn3.7 software and then visualized by VMD1.9.2 software.[70] The geometrical optimization, MEP analysis, interaction energy, and PoC-based calculations were performed using Gaussian09 software.[71]

3. Results and discussion

3.1. MEP and $V_{s,max}$ calculations

The molecular electrostatic potential (MEP) model is widely used for deducing the reactive sites on isolated monomers that can, in turn, provide potential sites for electrophilic or nucleophilic attacks.[72] Therefore, the MEP maps were generated at MP2/aug-cc-pVTZ (PP) level of theory for the studied monomers to ascertain the occurrence of σ-hole and R˙-hole regions. The $V_{s,max}$ values at the σ-hole, and R˙-hole were also estimated using Multiwfn3.5 software. The generated MEP maps and the estimated $V_{s,max}$ values for the studied monomers are illustrated in Fig. 2.

According to the data presented in Fig. 2, the studied tetrel-containing molecules exhibited variable-in-size σ-holes along the W–T bond extensions (where T = C, Si, and Ge, and W = H and F). The σ-hole size was increased with moving from lighter to heavier tetrel atoms in order C < Si < Ge. For example, the $V_{s,max}$ values at the σ-hole were found to be 31.6, 64.1, and 75.4 kcal mol^{-1} for F–C–F$_3$, F–Si–F$_3$, and F–Ge–F$_3$ molecules, respectively. As well, a direct correlation between the electronegativity of the W atom and σ-hole size of the tetrel atom was observed. Taking W–Ge–F$_3$ system as an example, the obtained $V_{s,max}$ values at the σ-hole for H–Ge–F$_3$, and F–Ge–F$_3$ were 48.5 and 75.4 kcal mol^{-1}, respectively.

Interestingly, a positive region opposite to the unpaired electron (i.e., R˙-hole) was noticed in the studied radicals. The $V_{s,max}$ magnitude at the R˙-hole attenuated in the order ˙GeF$_3$ >

˙SiF$_3$ > ˙CF$_3$ and obtained with values of 52.8, 51.2, and 30.9 kcal mol^{-1}, respectively. Generally, the $V_{s,max}$ values at the σ-hole were higher than those at R˙-hole for the same monomer.

3.2. PoC-based calculations

3.2.1. R˙-hole location.
To achieve the aim of the study, the optimum R˙-hole location for the studied ˙TF$_3$ radicals remained to be precisely determined. Based on a previous recommendation, $V_{s,max}$ calculations are unreliable in determining the location of the maximum positive electrostatic potential.[52] Therefore, the 2D-molecular stabilization energy surfaces were generated with the help of the PoC approach and depicted in Fig. 3.

As shown in Fig. 3, the largest molecular stabilization energies (i.e., more negative) were observed at the centroid of the F$_3$ atoms with values of −0.15, −0.30, and −0.31 kcal mol^{-1} for ˙CF$_3$, ˙SiF$_3$, and ˙GeF$_3$ radicals, respectively. These findings are in line with those for lp-hole containing molecules, where the precise lp-hole positions were identified at the centroid of the *xyz* plane in the covalently bonded Group V-VIII elements.[49]

3.2.2. Lewis basicity and acidity effects.
Towards scrutinizing the $^{\pm}$σ-hole and $^{\pm}$R˙-hole interactions from the electrostatic perspective, the Lewis basicity and acidity effects were elucidated with the incorporation of the PoC approach. Thence, the molecular stabilization energy curves for ˙TF$_3$ and W–T–F$_3$ monomers were generated at T···PoC distance in a range 2.5 to 5.0 Å along the σ-hole and R˙-hole extensions (see Fig. S1 and S2†). The molecular stabilization energy curves of carbon-containing molecules were taken as an example and compared in Fig. 4. Table 1 lists the values of molecular stabilization energies at T···PoC distance of 2.5 Å for the investigated monomers.

Concerning $^{-}$σ-hole and $^{-}$R˙-hole interactions, the molecular stabilization energies were boosted by increasing the negativity of PoCs (i.e., Lewis basicity) and decreasing the T···PoC distances. For example, the observed molecular stabilization energies for ˙CF$_3$ monomer were −0.65, −1.96, −5.06, and −14.5 kcal mol^{-1} at T···PoC distance of 2.5 Å in the presence of −0.10, −0.25, −0.50, and −1.00 au PoCs, respectively (see Table 1). Furthermore, the effect of Lewis basicity was most distinguishable for the F–T–F$_3$ followed in order by the ˙TF$_3$ and H–T–

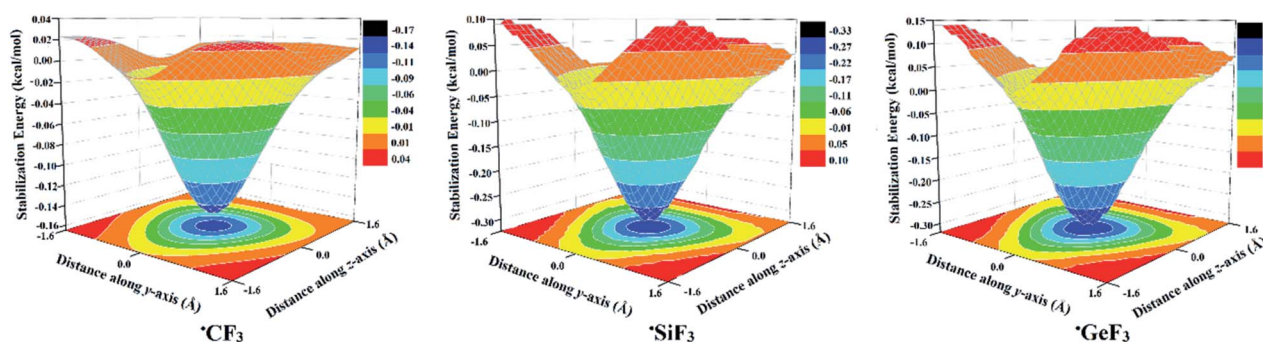**Fig. 3** Generated 2D-molecular stabilization energy surfaces for the investigated ˙CF$_3$, ˙SiF$_3$, and ˙GeF$_3$ monomers in the presence of −0.01 PoC at a T···PoC distance of 2.0 Å along the *x*-axis (see Computational methods section for details).
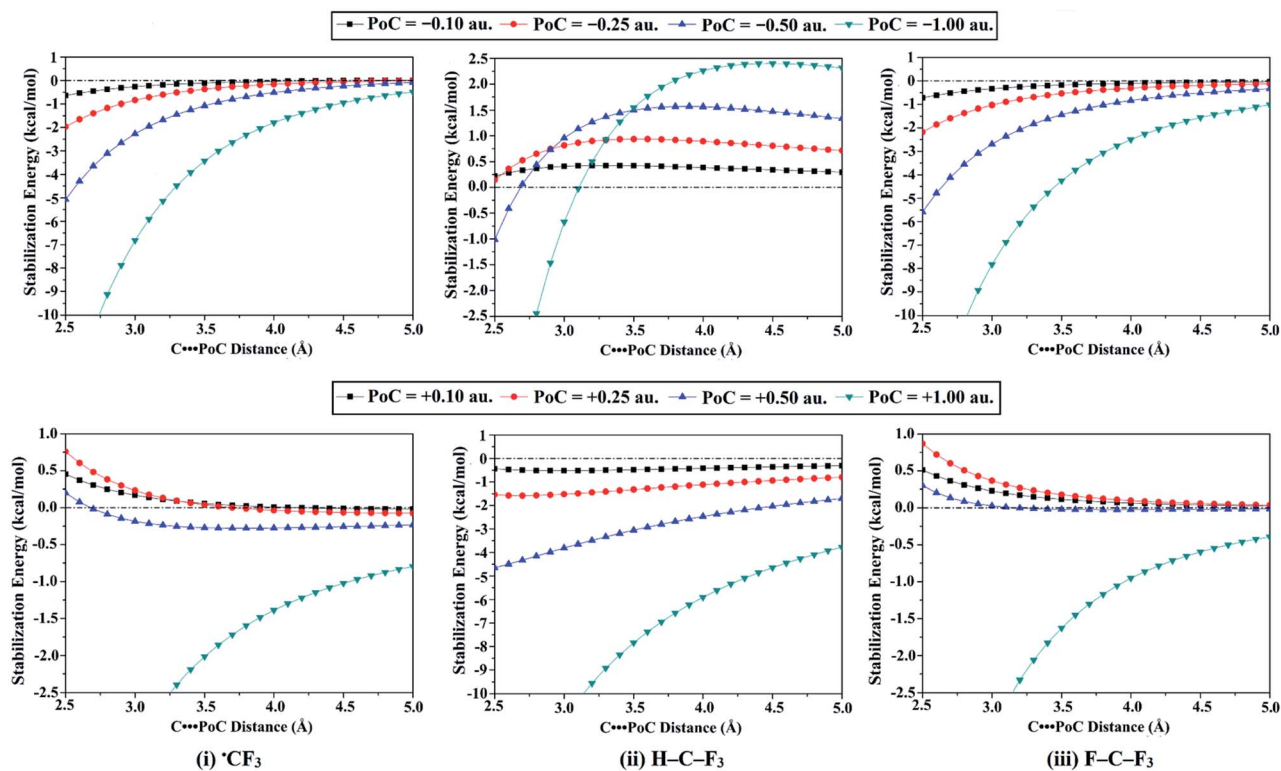
Fig. 4 Generated molecular stabilization energy curves for the (i) ·CF$_3$, (ii) H−C−F$_3$, and (iii) F−C−F$_3$ monomers in the presence of ±0.10, ±0.25, ±0.50, and ±1.00 au PoCs at T⋯PoC distances ranging from 2.5 Å to 5.0 Å.

F$_3$ systems. For instance, the obtained molecular stabilization energies at T⋯PoC distance of 2.5 Å for F−Ge−F$_3$, ·GeF$_3$, and H−Ge−F$_3$ monomers were −32.91, −21.92, and −19.71 kcal mol^{-1} in case of −1.00 au PoC, respectively. The observation can explain this pattern that the systematic growth of the $V_{s,max}$ magnitude at σ-hole, and R·-hole led to a gradual increase in the molecular stabilization energies (i.e., became more negative). More interestingly, according to Fig. 4, molecular stabilization energies remained to be observed at long T⋯PoC distances for ·CF$_3$ and F−C−F$_3$ molecules, demonstrating the dominance of the attractive electrostatic force between the negative PoC and the positive electrophilic sites over the tetrel atom (i.e., σ-hole and R·-hole). Otherwise, in the case of H−C−F$_3$ molecule, molecular destabilization energies were noticed and augmented by increasing the Lewis basicity, indicating the repulsive electrostatic interaction with F$_3$ atoms is the controlling one at long T⋯PoC distance.

For $^+$σ-hole and $^+$R·-hole interactions, molecular stabilization energies were observed for all investigated molecules, except SiF$_4$ and GeF$_4$. The incompetence of SiF$_4$ and GeF$_4$ to participate in $^+$σ-hole interaction is appertaining to the significant repulsive interaction between the positive PoC and the excessive positive σ-hole. For H−C−F$_3$ monomer as an exemplar, H−C−F$_3$ demonstrated molecular stabilization energies of −0.44, −1.54, −4.64, and −16.81 kcal mol^{-1} at T⋯PoC distance of 2.5 Å in the presence of +0.10, +0.25, +0.50, and +1.00 au PoCs, respectively. As claimed by the latter observation, the molecular stabilization energies boosted with increasing the

positivity of the PoC (i.e., Lewis acidity) despite the repulsive electrostatic interaction between the positive σ-hole and positive PoC, illustrating the effectual role of polarization in stabilizing such interactions. For some tetrel-containing molecules, generally, unfavorable electrostatic interactions were noticed at very short T⋯PoC distances. It is apparent from Table 1 that the H−T−F$_3$ system gave more favorable electrostatic interaction compared to ·TF$_3$ and F−T−F$_3$ systems. For instance, the molecular stabilization energies were found to increase in the order of F−C−F$_3$ < ·CF$_3$ < H−C−F$_3$ with values of −5.75, −6.07, and −16.81 kcal mol^{-1} at 2.5 Å in the presence of +1.00 au PoC, respectively.

Overall, with respect to the research question, it was found that the studied monomers can electrostatically interact with Lewis bases and acids along the R·-hole extension, forming $^±$R·-hole interactions. Compared with the $^-$σ-hole and –R·-hole interactions, the parallel $^+$σ-hole and $^+$R·-hole interactions with Lewis acids are less favorable. The substantial role of polarization effect and F$_3$ atoms in forming such interactions cannot be neglected.

3.3. Tetrel⋯B/R·/A complexes

3.3.1. Interaction energy. To affirm the potency of the studied monomers to participate in $^±$σ-hole and $^±$R·-hole interactions, geometrical optimization was performed for ·TF$_3$⋯ and W−T−F$_3$⋯B/R·/A complexes. The interaction energies were then estimated at MP2/aug-cc-pVTZ(PP) and CCSD(T)/CBS levels of theory (see Table 2).

Table 1 The molecular stabilization energies (in kcal mol^{-1}) of the studied $^{\bullet}TF_3$ and $W–T–F_3$ systems (where T = C, Si, and Ge, and W = H and F) in the presence of ±0.10, ±0.25, ±0.50, or ±1.00 au PoCs at a T···PoC distance of 2.5 Å

Molecule	Molecular stabilization energies (kcal mol^{-1}) at 2.5 Å			
	PoC = −0.10	PoC = −0.25	PoC = −0.50	PoC = −1.00
$^{\bullet}CF_3$	−0.65	−1.96	−5.06	−14.50
$H–C–F_3$	0.22	0.14	−1.01	−6.94
$F–C–F_3$	−0.72	−2.18	−5.58	−15.82
$^{\bullet}SiF_3$	−1.19	−3.47	−8.51	−22.96
$H–Si–F_3$	−1.10	−3.24	−8.03	−21.91
$F–Si–F_3$	−1.84	−5.06	−11.57	−28.62
$^{\bullet}GeF_3$	−0.20	−3.01	−7.73	−21.92
$H–Ge–F_3$	−0.76	−2.44	−6.61	−19.71
$F–Ge–F_3$	−2.21	−6.00	−13.55	−32.91

Molecule	Molecular stabilization energies (kcal mol^{-1}) at 2.5 Å			
	PoC = +0.10	PoC = +0.25	PoC = +0.50	PoC = +1.00
$^{\bullet}CF_3$	0.45	0.76	0.20	−5.75
$H–C–F_3$	−0.44	−1.54	−4.64	−16.81
$F–C–F_3$	0.51	0.87	0.30	−6.07
$^{\bullet}SiF_3$	0.92	1.77	1.62	−1.19
$H–Si–F_3$	0.83	1.53	1.12	−7.63
$F–Si–F_3$	1.59	3.46	5.12	1.23
$^{\bullet}GeF_3$	0.69	1.14	0.17	−10.22
$H–Ge–F_3$	0.46	0.55	−1.04	−12.88
$F–Ge–F_3$	1.93	4.30	6.67	3.74

As can be readily appreciated from Table 2, the investigated monomers exhibited a strong tendency to interact with Lewis bases, Lewis acids, and free radicals with CCSD(T)/CBS interaction energies in the range −0.03 to −17.83, 0.48 to −0.72, and −0.43 to −2.42 kcal mol^{-1}, respectively. For the analyzed complexes, the interaction energies were almost greater (*i.e.*, more negative) for the Ge-containing complexes compared to the Si and C counterparts, which are in agreement with the MEP results (see Fig. 2). Noteworthy, reasonable differences between the interaction energies estimated at MP2/aug-cc-pVTZ(PP) and those calculated at CCSD(T)/CBS were observed, demonstrating the accuracy and effectiveness of the MP2/aug-cc-pVTZ(PP) level of theory to investigate such non-covlanet interactions. This is in agreement with previous studies on estimating the strength of noncovlent interactions in related systems[28,32,73–76] (Table 2).

In regards to $^{\bullet}TF_3\cdots$ and $W–T–F_3\cdots B$ complexes, $^-\sigma$-hole, and $^-R^{\bullet}$-hole interaction energies were large negative values, indicating strong interactions between the interacting subunits. A linear correlation was found between the interaction energies and the $V_{s,max}$ at the σ-hole and R$^{\bullet}$-hole over the tetrel atom, where the interaction energies enhanced in order $H–T–F_3\cdots B$ < $^{\bullet}TF_3\cdots B$ < $F–T–F_3\cdots B$. For example, the CCSD(T)/CBS interaction energies for $H–Ge–F_3\cdots$, $^{\bullet}GeF_3\cdots$, and $F–Ge–F_3\cdots NCH$ complexes were noticed with values of −2.32, −2.95, and −17.83 kcal mol^{-1}, respectively. It was also found that the greater the atomic size of tetrel atom, the shorter T···B contact, which in turn resulted in strengthening interaction energies.

Table 2 Interaction energies (in kcal mol^{-1}) calculated at MP2/aug-cc-pVTZ(PP) and CCSD(T)/CBS levels of theory for the optimized $^{\bullet}TF_3\cdots$ and $W–T–F3\cdots B/R^{\bullet}/A$ complexes (where T = C, Si, and Ge, W = H and F, B = Lewis bases, R$^{\bullet}$ = free radicals, and A = Lewis acids), and T··· B/R$^{\bullet}$/A intermolecular distances (d, Å)

$^{\bullet}TF_3/W–T–F_3\cdots B$ systems						
	NCH			FH		
Complex	E_{MP2}	$E_{CCSD(T)}$	$d_{T\cdots NCH}$	E_{MP2}	$E_{CCSD(T)}$	$d_{T\cdots FH}$
$^{\bullet}CF_3\cdots B$	−1.04	−1.14	3.29	−0.58	−0.75	3.18
$H–C–F_3\cdots B$	0.01	−0.04	3.55	0.08	−0.03	3.39
$F–C–F_3\cdots B$	−1.09	−1.15	3.36	−0.62	−0.79	3.23
$^{\bullet}SiF_3\cdots B$	−2.08	−2.28	3.17	−0.77	−1.03	3.23
$H–Si–F_3\cdots B$	−1.95	−2.10	3.18	−0.70	−0.95	3.22
$F–Si–F_3\cdots B$	−3.44	−3.64	3.01	−1.37	−1.67	3.10
$^{\bullet}GeF_3\cdots B$	−2.70	−2.95	2.96	−0.56	−0.89	3.14
$H–Ge–F_3\cdots B$	−2.13	−2.32	3.01	−0.39	−0.67	3.21
$F–Ge–F_3\cdots B$	−10.21	−17.83	2.39	−1.84	−2.29	2.95

$^{\bullet}TF_3/W–T–F_3\cdots R^{\bullet}$ systems						
	$^{\bullet}CH_3$			$^{\bullet}CF_3$		
Complex	E_{MP2}	$E_{CCSD(T)}$	$d_{T\cdots CH_3}$	E_{MP2}	$E_{CCSD(T)}$	$d_{T\cdots CF_3}$
$^{\bullet}CF_3\cdots R^{\bullet}$	−0.41	−0.57	3.74	−0.27	−0.47	3.55
$H–C–F_3\cdots R^{\bullet}$	−0.26	−0.43	3.86	−0.56	−0.78	3.52
$F–C–F_3\cdots R^{\bullet}$	−0.46	−0.63	3.75	−0.34	−0.50	3.53
$^{\bullet}SiF_3\cdots R^{\bullet}$	−0.69	−0.98	3.65	−0.37	−0.65	3.58
$H–Si–F_3\cdots R^{\bullet}$	−0.72	−1.02	3.61	−0.42	−0.73	3.52
$F–Si–F_3\cdots R^{\bullet}$	−1.03	−1.40	3.47	−0.25	−0.54	3.47
$^{\bullet}GeF_3\cdots R^{\bullet}$	−0.74	−1.19	3.47	−0.35	−0.85	3.36
$H–Ge–F_3\cdots R^{\bullet}$	−0.70	−1.11	3.52	−0.51	−0.97	3.39
$F–Ge–F_3\cdots R^{\bullet}$	−1.79	−2.42	3.17	−0.19	−0.64	3.25

$^{\bullet}TF_3/W–T–F_3\cdots A$ systems						
	HCN			HF		
Complex	E_{MP2}	$E_{CCSD(T)}$	$d_{T\cdots HCN}$	E_{MP2}	$E_{CCSD(T)}$	$d_{T\cdots HF}$
$^{\bullet}CF_3\cdots A$	0.07	0.02	2.96	0.11	0.09	3.49
$H–C–F_3\cdots A$	−1.07	−1.14	2.88	−0.79	−0.88	2.91
$F–C–F_3\cdots A$	0.00	−0.03	2.99	0.15	0.14	3.26
$^{\bullet}SiF_3\cdots A$	−0.14	−0.16	3.41	0.07	0.04	3.97
$H–Si–F_3\cdots A$	−0.18	−0.22	3.53	−0.08	−0.09	4.62
$F–Si–F_3\cdots A$	0.49	0.48	3.55	—[a]	—[a]	—[a]
$^{\bullet}GeF_3\cdots A$	−0.34	−0.46	3.14	−0.01	−0.07	3.46
$H–Ge–F_3\cdots A$	−0.58	−0.72	3.10	−0.28	−0.34	3.57
$F–Ge–F_3\cdots A$	0.44	0.43	3.86	—[a]	—[a]	—[a]

[a] Optimized structure could not be obtained.

The example given was for $F–C–F_3\cdots$, $F–Si–F_3\cdots$, and $F–Ge–F_3\cdots$ NCH complexes, where the CCSD(T)/CBS interaction energies were noticed with values of −1.15, −3.64, and −17.83 kcal mol^{-1} at T···N intermolecular distances values of 3.36, 3.01, and 2.39 Å, respectively (see Table 2). Moreover, the NCH Lewis base was found to interact more strongly than the FH candidate with the studied monomers.

For $^{\bullet}TF_3\cdots$ and $W–T–F_3\cdots A$ complexes, favorable $^+\sigma$-hole and $^+R^{\bullet}$-hole interactions were observed for most of the studied

Table 3 The estimated SAPT0 interaction energy and its components (in kcal mol^{-1}) for the $^\bullet$TF$_3\cdots$ and W−T−F$_3\cdots$B/R$^\bullet$/A complexes (where T = C, Si, and Ge, W = H and F, B = Lewis bases, R$^\bullet$ = free radicals, and A = Lewis acids)

$^\bullet$TF$_3$/W−T−F$_3\cdots$B systems

Complex	NCH					FH				
	E_{elst}	E_{exch}	E_{ind}	E_{disp}	E_{int}^{SAPT0}	E_{elst}	E_{exch}	E_{ind}	E_{disp}	E_{int}^{SAPT0}
$^\bullet$CF$_3\cdots$B	−1.26	1.77	−0.22	−1.63	−1.34	−0.54	0.81	−0.11	−0.98	−0.82
H−C−F$_3\cdots$B	0.22	0.92	−0.14	−1.19	−0.19	0.30	0.48	−0.08	−0.76	−0.04
F−C−F$_3\cdots$B	−1.37	1.58	−0.21	−1.57	−1.55	−0.67	0.77	−0.11	−0.97	−0.98
$^\bullet$SiF$_3\cdots$B	−3.50	3.76	−0.67	−2.42	−2.83	−1.04	1.10	−0.21	−1.11	−1.26
H−Si−F$_3\cdots$B	−3.35	3.65	−0.64	−2.39	−2.72	−1.01	1.12	−0.21	−1.13	−1.23
F−Si−F$_3\cdots$B	−6.13	5.66	−1.24	−2.97	−4.68	−2.04	1.51	−0.35	−1.29	−2.17
$^\bullet$GeF$_3\cdots$B	−6.12	7.20	−1.56	−3.63	−4.11	−1.22	1.71	−0.32	−1.44	−1.28
H−Ge−F$_3\cdots$B	−5.16	6.42	−1.26	−3.42	−3.41	−0.84	1.37	−0.25	−1.30	−1.02
F−Ge−F$_3\cdots$B	−24.0	28.45	−12.1	−7.75	−15.4	−3.28	2.57	−0.72	−1.76	−3.19

$^\bullet$TF$_3$/W−T−F$_3\cdots$R$^\bullet$ systems

Complex	$^\bullet$CH$_3$					$^\bullet$CF$_3$				
	E_{elst}	E_{exch}	E_{ind}	E_{disp}	E_{int}^{SAPT0}	E_{elst}	E_{exch}	E_{ind}	E_{disp}	E_{int}^{SAPT0}
$^\bullet$CF$_3\cdots$R$^\bullet$	−0.66	1.12	−0.06	−1.01	−0.61	−0.27	1.07	−0.08	−1.17	−0.45
H−C−F$_3\cdots$R$^\bullet$	−0.36	0.93	−0.06	−0.95	−0.44	−0.86	1.46	−0.12	−1.41	−0.94
F−C−F$_3\cdots$R$^\bullet$	−0.72	1.18	−0.06	−1.05	−0.66	−0.25	1.25	−0.10	−1.30	−0.41
$^\bullet$SiF$_3\cdots$R$^\bullet$	−1.43	2.07	−0.18	−1.46	−1.01	−0.33	1.48	−0.17	−1.46	−0.46
H−Si−F$_3\cdots$R$^\bullet$	−1.53	2.25	−0.20	−1.55	−1.03	−0.42	1.72	−0.20	−1.58	−0.48
F−Si−F$_3\cdots$R$^\bullet$	−2.33	3.11	−0.39	−1.82	−1.43	0.03	1.91	−0.29	−1.65	−0.06
$^\bullet$GeF$_3\cdots$R$^\bullet$	−2.31	3.65	−0.40	−2.20	−1.26	−1.01	3.21	−0.42	−2.38	−0.60
H−Ge−F$_3\cdots$R$^\bullet$	−2.02	3.26	−0.32	−2.07	−1.15	−1.05	2.96	−0.36	−2.28	−0.73
F−Ge−F$_3\cdots$R$^\bullet$	−4.68	6.60	−1.47	−3.01	−2.57	−0.20	3.56	−0.75	−2.46	0.14

$^\bullet$TF$_3$/W−T−F$_3\cdots$A systems

Complex	HCN					HF				
	E_{elst}	E_{exch}	E_{ind}	E_{disp}	E_{int}^{SAPT0}	E_{elst}	E_{exch}	E_{ind}	E_{disp}	E_{int}^{SAPT0}
$^\bullet$CF$_3\cdots$A	0.65	0.45	−0.24	−0.81	0.05	0.40	0.03	−0.09	−0.21	0.13
H−C−F$_3\cdots$A	−0.60	0.81	−0.35	−1.06	−1.21	−0.12	0.39	−0.33	−0.66	−0.72
F−C−F$_3\cdots$A	0.82	0.44	−0.25	−0.83	0.19	0.75	0.08	−0.15	−0.34	0.35
$^\bullet$SiF$_3\cdots$A	0.36	0.10	−0.14	−0.44	−0.11	0.29	0.01	−0.06	−0.14	0.10
H−Si−F$_3\cdots$A	0.43	0.14	−0.16	−0.51	−0.10	0.02	0.01	−0.03	−0.06	−0.06
F−Si−F$_3\cdots$A	1.18	0.07	−0.13	−0.39	0.74	—^{a}	—^{a}	—^{a}	—^{a}	—^{a}
$^\bullet$GeF$_3\cdots$A	0.41	0.49	−0.30	−0.91	−0.31	0.53	0.08	−0.16	−0.34	0.10
H−Ge−F$_3\cdots$A	0.23	0.56	−0.33	−0.97	−0.51	0.21	0.05	−0.13	−0.29	−0.16
F−Ge−F$_3\cdots$A	1.03	0.03	−0.08	−0.27	0.67	—^{a}	—^{a}	—^{a}	—^{a}	—^{a}

^{a} Optimized structure could not be obtained, so no SAPT calculations were performed.

complexes. The inability of some monomers to engage in favorable interactions with Lewis acids can be attributed to the dominance of the repulsive electrostatic interaction between the electrophilic site over the tetrel atom and the Lewis acid. Generally, the interaction energies reinforced by decreasing the $V_{s,max}$ value over the tetrel atom in the order F−T−F$_3\cdots$A < $^\bullet$TF$_3\cdots$A < H−T−F$_3\cdots$A. As an exemplar, the CCSD(T)/CBS interaction energies were found with values of 0.43, −0.46, and −0.72 kcal mol^{-1} for F−Ge−F$_3\cdots$, $^\bullet$GeF$_3\cdots$, and H−Ge−F$_3\cdots$HCN complexes, respectively. However, the CCSD(T)/CBS interaction energies for $^\bullet$CF$_3\cdots$, $^\bullet$SiF$_3\cdots$ and $^\bullet$GeF$_3\cdots$HCN complexes were with values of 0.02, −0.16, and −0.46 kcal mol^{-1}, respectively,

despite increasing the $V_{s,max}$ at R$^\bullet$-hole in order of C < Si < Ge. These findings explicitly referred to the interaction of F$_3$ atoms with the H atom of the Lewis acid and were further investigated by NCI analysis. Compared to HF-containing complexes, the interaction energies for HCN-containing complexes were systematically larger (*i.e.*, more negative). For example, the CCSD(T)/CBS interaction energies for H−Ge−F$_3\cdots$HCN and $\cdots$HF complexes were −0.72 and −0.34 kcal mol^{-1}, respectively.

In the case of $^\bullet$TF$_3\cdots$ and W−T−F$_3\cdots$R$^\bullet$ complexes, which exhibited a staggered conformation with C$_{3v}$ symmetry, the $^\bullet$CH$_3$, and $^\bullet$CF$_3$ can act as a nucleophile and an electrophile, respectively, according to the generated MEP maps (see
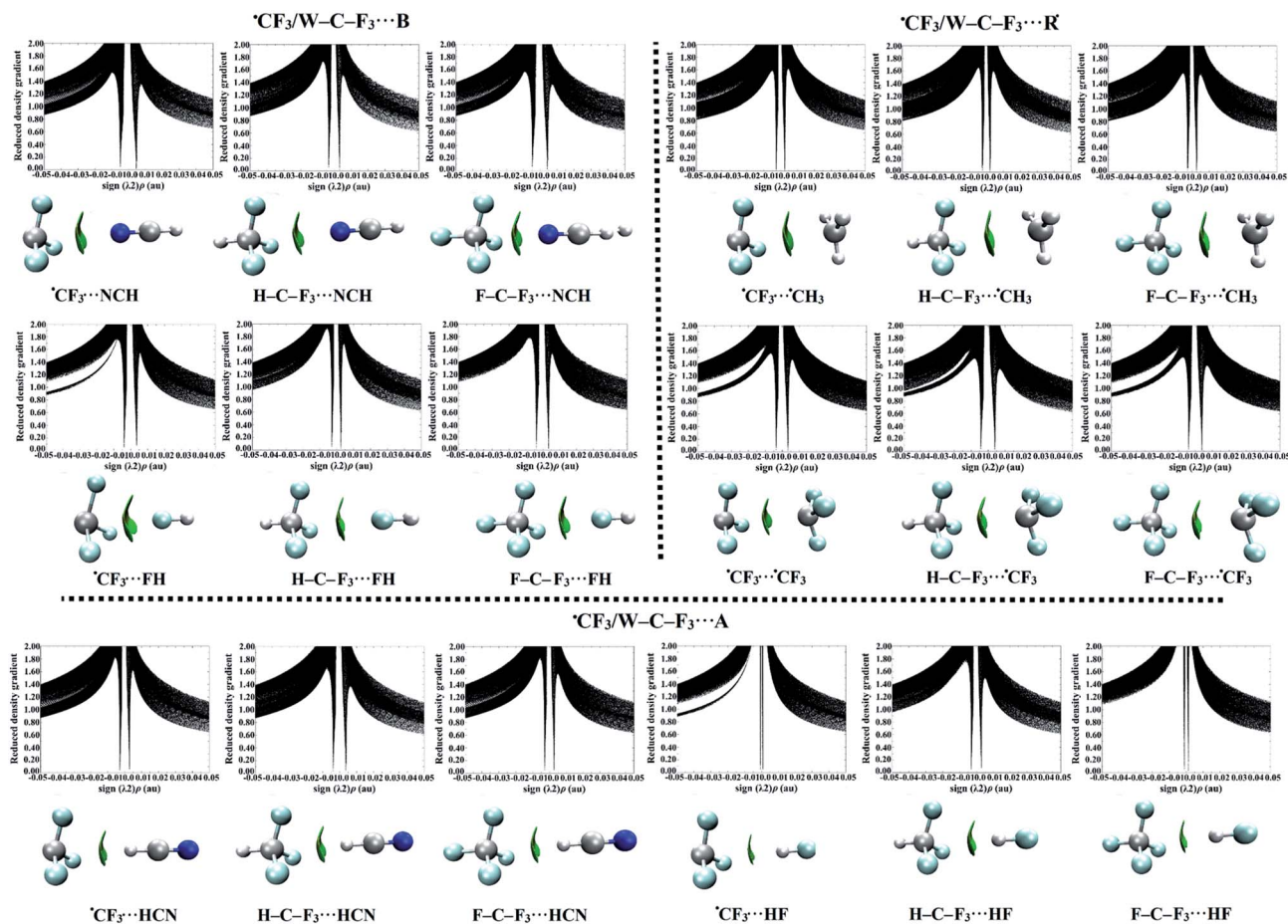
Fig. 5 NCI isosurfaces of the studied ˙CF₃··· and W−C−F₃···B/R˙/A complexes (where W = H and F, B = Lewis bases, R˙ = free radicals, and A = Lewis acids). NCI isosurfaces are colored on a blue–green–red (BGR) scale with blue and red for attractive and repulsive interactions, respectively. The corresponding sign (λ₂)ρ *vs.* RDG plots to the NCI isosurfaces are also depicted.

Fig. S3†). For ˙TF₃··· and W−T−F₃···˙CH₃ complexes, the interaction energies increased in the same order as in Lewis base-containing complexes, confirming the potentiality of ˙CH₃ to act as a Lewis base. For instance, the CCSD(T)/CBS interaction energies amounted to −1.11, −1.19, and −2.42 kcal mol⁻¹ for H−Ge−F₃···, ··GeF₃···, and F−Ge−F₃···˙CH₃ complexes, respectively. On the other hand, for ˙CF₃-containing complexes, the interaction became stronger in the order F−T−F₃···˙CF₃ < ˙TF₃··· ˙CF₃ < H−T−F₃···˙CF₃, demonstrating that ˙CF₃ could act as a Lewis acid. As an example, the CCSD(T)/CBS interaction energies were observed with values of −0.64, −0.85, and −0.97 kcal mol⁻¹ for F−Ge−F₃···, ˙GeF₃···, and H−Ge−F₃···˙CF₃ complexes, respectively (see Table 2).

Overall, these results divulge that the strength of ±σ-hole interactions is higher compared to the ±R˙-hole ones, and the most stable complexes were observed for the ones containing Lewis bases. Besides, the strength of ±σ-hole and ±R˙-hole interactions in ˙TF₃··· and W−T−F₃···B/R˙/A complexes is not exclusive to the repulsive/attractive electrostatic interaction between the electrophilic site on tetrel atom and B/R˙/A, but also the interactions with the F₃ atoms. These appealing findings seem to be consistent with other previous reports concerning the interactions of tetrel-containing molecules with Lewis bases, acids, and free radicals.[28,30,36,74,77,78]

3.3.2. SAPT-EDA calculation. To elucidate the nature of ±σ-hole and ±R˙-hole interactions, symmetry adapted perturbation theory-based energy decomposition analysis (SAPT-EDA) was applied. SAPT-EDA partitions the interaction energy into four components; electrostatics (E_{elst}), exchange (E_{exch}), induction (E_{ind}), and dispersion (E_{disp}). These components and the total SAPT0 interaction energy for the ˙TF₃··· and W−T−F₃···B/R˙/A complexes were estimated and presented in Table 3.

A perusal of the data in Table 3 shows that for ⁻σ-hole and ⁻R˙-hole interactions, the E_{disp}, E_{elst}, and E_{ind} terms are negative, unlikely; the E_{exch} is positive. As well, all these terms increased in the order C < Si < Ge. Generally, it is apparent that the E_{disp} governs the ⁻σ-hole and ⁻R˙-hole interactions, followed by the E_{elst}, and E_{ind}. For instance, E_{disp} contributions were 89, 90, and 69% out of the total attractive terms for the H−C−F₃···NCH, ···FH, and ···˙CH₃ complexes, respectively. On the other hand, for Ge-containing molecules interacting with NCH as Lewis base, the interactions were dominated by E_{elst}; where the E_{elst} contribution to the total interaction energy ranged from −5.16 to −24.0 kcal mol⁻¹ and the E_{disp} contribution ranged

from -3.42 to -7.75 kcal mol^{-1} (see Table 3). These findings demonstrated the importance of electrostatic and dispersion energies in stabilizing ˙TF$_3$··· and W–T–F3···NCH/FH/˙CH$_3$ complexes.

Turning now to $^+$σ-hole and $^+$R˙-hole interactions, the E_{disp} term was the most important attractive contributor. Besides, generally, the E_{elst} and E_{ind} terms help in promoting the strength of interactions for ˙TF$_3$/W–T–F$_3$···CF$_3$ and ···HCN/HF complexes, respectively. For example, the E_{disp}, E_{elst}, and E_{ind} were -2.38, -1.01, and -0.42 kcal mol^{-1} for ˙GeF$_3$···˙CF$_3$ complex, respectively (see Table 3).

Taken together, these results disclose that the stability of the studied complexes-containing Lewis bases, Lewis acids, and radicals are attributed mainly to the dispersion forces, with enhanced contributions from electrostatic and induction forces.

3.3.3. RDG–NCI analysis. To reveal the characteristics and nature of $^\pm$σ-hole and $^\pm$R˙-hole interactions, NCI calculations were carried out for the optimized ˙TF$_3$··· and W–T–F$_3$···B/R˙/A complexes. NCI isosurfaces and plots of the reduced density gradient (RDG) *versus* the electron density (ρ) multiplied by the sign of the second Hessian eigenvalue (λ_2) of the analyzed complexes were generated at MP2/aug-cc-pVTZ (PP) level of theory and presented in Fig. S4 and S5,† respectively. The RDG–NCI plots of carbon-containing complexes were represented in Fig. 5, as an example.

The results obtained from the NCI isosurfaces demonstrated the favorable $^-$σ-hole and $^-$R˙-hole interactions, showing disc-shaped green isosurfaces between the interacting fragments (Fig. S4†). Besides, the green isosurfaces became larger with increasing interaction strength, converting to blue ones for the strong interactions as observed in the F–Ge–F$_3$···NCH complex. Moreover, the corresponding spikes of sign $(\lambda_2)\rho$ at low densities confirmed the existence of such attractive interactions (sign $(\lambda_2)\rho < 0$). The location of spikes had a greater deviation from zero, and its shape became broader with enhancing the interaction energy (see Fig. S5†).

For $^+$σ-hole and $^+$R˙-hole interactions, disc-shaped green isosurfaces were also noticed for the studied complexes, asserting the existence of such interactions (see Fig. S4†). Furthermore, green isosurfaces were observed between the F$_3$ atoms and Lewis acids, revealing their role in stabilizing the Lewis acids-containing complexes. The favorable interactions were also characterized by spikes at the negative sign $(\lambda_2)\rho$. For instance, the spikes corresponding to each of H–C–F$_3$···HCN and ···˙CF$_3$ complexes were located at negative sign $(\lambda_2)\rho$, indicating the probability of such interactions to dwell (see Fig. S5†).

In summary, these findings underlined that the $^-$σ-hole and $^-$R˙-hole interactions are the most favorable ones, where the large green isosurfaces and broad spikes were observed in their complexes.

4. Conclusion

The potentiality of the tetrel-containing molecules to engage in interactions with Lewis bases, free radicals, and Lewis acids along the R˙-hole extension, forming $^\pm$R˙-hole interactions, was uncovered for the first time. The characteristics of $^\pm$R˙-hole

interactions were compared to the $^\pm$σ-hole analogs in ˙TF$_3$··· and W–T–F$_3$···B/R˙/A complexes, respectively. The nature and characteristics of such interactions were discussed adequately by interpreting the MEP, $V_{s,max}$, PoC, interaction energy, SAPT, and NCI-based results. These findings suggested that (i) the occurrence of σ-hole and R˙-hole over the tetrel atom was conspicuous, (ii) utilizing the PoC approach, the ability of the ˙TF$_3$··· and W–T–F$_3$ monomers to participate in favorable electrostatic interaction with Lewis bases and acids was demonstrated, (iii) the highest molecular stabilization energies were obtained in case of ±1.00 au PoC due to the effectual role of polarization, (iv) ˙TF$_3$ and W–T–F$_3$ monomers showed more favorable interactions with Lewis bases than Lewis acids, (v) a comparison of the $^\pm$σ-hole and $^\pm$R˙-hole interactions revealed the former is more energetically favorable, (vi) the strength of such interactions is not exclusive to the repulsive/attractive electrostatic interaction between the electrophilic site on tetrel atom and B/R˙/A, but also the interactions with the F$_3$ atoms, (vii) generally, the dispersion force played a critical role in stabilizing the tetrel-containing complexes, with a non-neglectable contribution of the electrostatic and induction forces to the interactions with Lewis bases and acids, respectively, and (viii) disc-shaped green isosurfaces were noticed between the interacting fragments, providing evidence of the presence of $^\pm$σ-hole and $^\pm$R˙-hole interactions. Thus, the upshot of these results adds to the growing body of research and will also be advantageous to the ones related to the crystal engineering and materials science fields.

Conflicts of interest

There are no conflicts to declare.

Acknowledgements

References

1 J. Y. C. Lim and P. D. Beer, *Chem*, 2018, **4**, 731–783.
2 J. Lee, L. M. Lee, Z. Arnott, H. Jenkins, J. F. Britten and I. Vargas-Baca, *New J. Chem.*, 2018, **42**, 10555–10562.
3 K. T. Mahmudov, M. N. Kopylovich, M. F. C. Guedes da Silva and A. J. L. Pombeiro, *Dalton Trans.*, 2017, **46**, 10121–10138.
4 G. Berger, K. Robeyns, J. Soubhye, R. Wintjens and F. Meyer, *CrystEngComm*, 2016, **18**, 683–690.
5 K. Kriz, J. Fanfrlik and M. Lepsik, *ChemPhysChem*, 2018, **19**, 2540–2548.
6 M. R. Scholfield, C. M. Zanden, M. Carter and P. S. Ho, *Protein Sci.*, 2013, **22**, 139–152.
7 P. Politzer, P. Lane, M. C. Concha, Y. Ma and J. S. Murray, *J. Mol. Model.*, 2007, **13**, 305–311.
8 T. Clark, M. Hennemann, J. S. Murray and P. Politzer, *J. Mol. Model.*, 2007, **13**, 291–296.
9 V. Angarov and S. Kozuch, *New J. Chem.*, 2018, **42**, 1413–1422.

10 A. Bauzá and A. Frontera, *Coord. Chem. Rev.*, 2020, **404**, 213112.

11 D. Quinonero, *Phys. Chem. Chem. Phys.*, 2017, **19**, 15530–15540.

12 W. Dong, X. Yang, J. Cheng, W. Li and Q. Li, *J. Fluorine Chem.*, 2018, **207**, 38–44.

13 D. Sethio, V. Oliveira and E. Kraka, *Molecules*, 2018, **23**, 2763–2783.

14 J. E. Del Bene, I. Alkorta, G. Sanchez-Sanz and J. Elguero, *J. Phys. Chem. A*, 2011, **115**, 13724–13731.

15 G. Sanchez-Sanz, C. Trujillo, I. Alkorta and J. Elguero, *Phys. Chem. Chem. Phys.*, 2014, **16**, 15900–15909.

16 A. Franconetti, D. Quinonero, A. Frontera and G. Resnati, *Phys. Chem. Chem. Phys.*, 2019, **21**, 11313–11319.

17 P. R. Varadwaj, *Molecules*, 2019, **24**, 3166–3183.

18 M. A. A. Ibrahim, A. A. M. Hasb and G. A. H. Mekhemer, *Theor. Chem. Acc.*, 2018, **137**, 38–47.

19 G. Cavallo, P. Metrangolo, R. Milani, T. Pilati, A. Priimagi, G. Resnati and G. Terraneo, *Chem. Rev.*, 2016, **116**, 2478–2601.

20 A. Bauza and A. Frontera, *Angew. Chem., Int. Ed. Engl.*, 2015, **54**, 7340–7343.

21 M. D. Esrafili and F. Mohammadian-Sabet, *Chem. Phys. Lett.*, 2016, **654**, 23–28.

22 L. Brammer, *Faraday Discuss.*, 2017, **203**, 485–507.

23 P. Varadwaj, A. Varadwaj, H. Marques and K. Yamashita, *Computation*, 2018, **6**, 51–84.

24 A. Varadwaj, H. M. Marques and P. R. Varadwaj, *Molecules*, 2019, **24**, 379–407.

25 A. Bauza, T. J. Mooibroek and A. Frontera, *Angew. Chem., Int. Ed. Engl.*, 2013, **52**, 12317–12321.

26 D. Mani and E. Arunan, *J. Phys. Chem. A*, 2014, **118**, 10081–10089.

27 G. Mahmoudi, A. Bauza, M. Amini, E. Molins, J. T. Mague and A. Frontera, *Dalton Trans.*, 2016, **45**, 10708–10716.

28 S. J. Grabowski, *Phys. Chem. Chem. Phys.*, 2014, **16**, 1824–1834.

29 C. Wang, Y. Aman, X. Ji and Y. Mo, *Phys. Chem. Chem. Phys.*, 2019, **21**, 11776–11784.

30 M. A. A. Ibrahim, A. H. M. Mahmoud and N. A. M. Moussa, *Chem. Pap.*, 2020, **74**, 3569–3580.

31 M. Liu, Q. Li and S. Scheiner, *Phys. Chem. Chem. Phys.*, 2017, **19**, 5550–5559.

32 M. Liu, Q. Li, J. Cheng, W. Li and H. B. Li, *J. Chem. Phys.*, 2016, **145**, 224310–224317.

33 M. D. Esrafili and P. Mousavian, *Molecules*, 2018, **23**, 2642–2661.

34 H. Xu, J. Cheng, X. Yang, Z. Liu, W. Li and Q. Li, *ChemPhysChem*, 2017, **18**, 2442–2450.

35 S. J. Grabowski, *Molecules*, 2018, **23**, 1183–1198.

36 Q. Li, X. Guo, X. Yang, W. Li, J. Cheng and H. B. Li, *Phys. Chem. Chem. Phys.*, 2014, **16**, 11617–11625.

37 Y. H. Wang, J. W. Zou, Y. X. Lu, Q. S. Yu and H. P. Xu, *Int. J. Quantum Chem.*, 2007, **107**, 501–506.

38 T. Clark, *J. Phys. Chem. A*, 2019, **123**, 3326–3333.

39 I. Alkorta, J. Elguero and M. Solimannejad, *J. Phys. Chem. A*, 2014, **118**, 947–953.

40 M. D. Esrafili and F. Mohammadian-Sabet, *J. Mol. Model.*, 2015, **21**, 65–73.

41 M. D. Esrafili, F. Mohammadian-Sabet and M. Solimannejad, *Chem. Phys. Lett.*, 2016, **659**, 196–202.

42 Z. Rezaei, M. Solimannejad and M. D. Esrafili, *Comput. Theor. Chem.*, 2015, **1074**, 101–106.

43 Q. Z. Li, R. Li, S. C. Yi, W. Z. Li and J. B. Cheng, *Struct. Chem.*, 2012, **23**, 411–416.

44 K. Boubekeur, J.-L. Syssa-Magalé, P. Palvadeau and B. Schöllhorn, *Tetrahedron Lett.*, 2006, **47**, 1249–1252.

45 M. Valko, D. Leibfritz, J. Moncol, M. T. Cronin, M. Mazur and J. Telser, *Int. J. Biochem. Cell Biol.*, 2007, **39**, 44–84.

46 R. W. Walker, *Sci. Prog.*, 1990, **74**, 163–187.

47 F. Olscher, I. Gottker-Schnetmann, V. Monteil and S. Mecking, *J. Am. Chem. Soc.*, 2015, **137**, 14819–14828.

48 A. Phaniendra, D. B. Jestadi and L. Periyasamy, *Indian J. Clin. Biochem.*, 2015, **30**, 11–26.

49 M. A. A. Ibrahim and E. M. Z. Telb, *ChemistrySelect*, 2019, **4**, 5489–5495.

50 M. A. A. Ibrahim and E. M. Z. Telb, *ACS Omega*, 2020, **5**, 21631–21640.

51 A. Bauza, T. J. Mooibroek and A. Frontera, *ChemPhysChem*, 2016, **17**, 1608–1614.

52 M. A. A. Ibrahim and N. A. M. Moussa, *ACS Omega*, 2020, **5**, 21824–21835.

53 M. A. A. Ibrahim and M. E. A. Safy, *Phosphorus, Sulfur Silicon Relat. Elem.*, 2019, **194**, 444–454.

54 M. A. A. Ibrahim, O. A. M. Ahmed, N. A. M. Moussa, S. El-Taher and H. Moustafa, *RSC Adv.*, 2019, **9**, 32811–32820.

55 M. A. A. Ibrahim, N. A. M. Moussa and M. E. A. Safy, *J. Mol. Model.*, 2018, **24**, 219.

56 M. A. A. Ibrahim, A. s. S. M. Rady, J. H. Al-Fahemi, E. M. Z. Telb, S. A. Ahmed, A. M. Shawky and N. A. M. Moussa, *ChemistrySelect*, 2020, **5**, 13223–13231.

57 C. Møller and M. S. Plesset, *Phys. Rev.*, 1934, **46**, 618–622.

58 D. E. Woon and T. H. Dunning, *J. Chem. Phys.*, 1994, **100**, 2975–2988.

59 D. E. Woon and T. H. Dunning, *J. Chem. Phys.*, 1993, **98**, 1358–1371.

60 M. A. A. Ibrahim, *J. Mol. Model.*, 2012, **18**, 4625–4638.

61 T. Lu and F. Chen, *J. Comput. Chem.*, 2012, **33**, 580–592.

62 S. F. Boys and F. Bernardi, *Mol. Phys.*, 1970, **19**, 553–566.

63 B. K. Mishra, S. Karthikeyan and V. Ramanathan, *J. Chem. Theory Comput.*, 2012, **8**, 1935–1942.

64 B. Jeziorski, R. Moszynski and K. Szalewicz, *Chem. Rev.*, 1994, **94**, 1887–1930.

65 J. M. Turney, A. C. Simmonett, R. M. Parrish, E. G. Hohenstein, F. A. Evangelista, J. T. Fermann, B. J. Mintz, L. A. Burns, J. J. Wilke, M. L. Abrams, N. J. Russ, M. L. Leininger, C. L. Janssen, E. T. Seidl, W. D. Allen, H. F. Schaefer, R. A. King, E. F. Valeev, C. D. Sherrill and T. D. Crawford, *Wiley Interdiscip. Rev.: Comput. Mol. Sci.*, 2012, **2**, 556–565.

66 E. G. Hohenstein and C. D. Sherrill, *J. Chem. Phys.*, 2010, **132**, 184111–184120.

67 E. G. Hohenstein, R. M. Parrish, C. D. Sherrill, J. M. Turney and H. F. Schaefer, 3rd, *J. Chem. Phys.*, 2011, **135**, 174107–174119.

68 J. F. Gonthier and C. D. Sherrill, *J. Chem. Phys.*, 2016, **145**, 134106–134116.

69 E. R. Johnson, S. Keinan, P. Mori-Sanchez, J. Contreras-Garcia, A. J. Cohen and W. Yang, *J. Am. Chem. Soc.*, 2010, **132**, 6498–6506.

70 W. Humphrey, A. Dalke and K. Schulten, *J. Mol. Graph.*, 1996, **14**, 33–38.

71 M. J. Frisch, G. W. Trucks, H. B. Schlegel, G. E. Scuseria, M. A. Robb, J. R. Cheeseman, G. Scalmani, V. Barone, B. Mennucci, G. A. Petersson, H. Nakatsuji, M. Caricato, X. Li, H. P. Hratchian, A. F. Izmaylov, J. Bloino, G. Zheng, J. L. Sonnenberg, M. Hada, M. Ehara, K. Toyota, R. Fukuda, J. Hasegawa, M. Ishida, T. Nakajima, Y. Honda, O. Kitao, H. Nakai, T. Vreven, J. A. Montgomery, J. E. Peralta, F. Ogliaro, M. Bearpark, J. J. Heyd, E. Brothers, K. N. Kudin, V. N. Staroverov, R. Kobayashi, J. Normand, K. Raghavachari, A. Rendell, J. C. Burant, S. S. Iyengar, J. Tomasi, M. Cossi, N. Rega, J. M. Millam, M. Klene, J. E. Knox, J. B. Cross, V. Bakken, C. Adamo, J. Jaramillo, R. Gomperts, R. E. Stratmann, O. Yazyev, A. J. Austin, R. Cammi, C. Pomelli, J. W. Ochterski, R. L. Martin, K. Morokuma, V. G. Zakrzewski, G. A. Voth, P. Salvador, J. J. Dannenberg, S. Dapprich, A. D. Daniels, Ö. Farkas, J. B. Foresman, J. V. Ortiz, J. Cioslowski and D. J. Fox, *Gaussian 09 Revision E01*, Gaussian Inc., Wallingford CT, USA, 2009.

72 P. K. Weiner, R. Langridge, J. M. Blaney, R. Schaefer and P. A. Kollman, *Proc. Natl. Acad. Sci. U. S. A.*, 1982, **79**, 3754–3758.

73 S. Grabowski, *Crystals*, 2017, **7**, 43–56.

74 M. Hou, Y. Zhu, Q. Li and S. Scheiner, *ChemPhysChem*, 2020, **21**, 212–219.

75 M. D. Esrafili, S. Asadollahi and P. Mousavian, *Chem. Phys. Lett.*, 2018, **691**, 394–400.

76 S. J. Grabowski, *Appl. Organomet. Chem.*, 2017, **31**, e3727–3736.

77 Y. X. Wei, J. B. Cheng, W. Z. Li and Q. Z. Li, *RSC Adv.*, 2017, **7**, 46321–46328.

78 S. J. Grabowski, *Struct. Chem.*, 2019, **30**, 1141–1152.